Preliminary Results of the Cloud Observation with CRL Airborne Cloud Profiling Radar (SPIDER)

Hiroaki Horie*, Hajime Okamoto, Suginori Iwasaki, Hiroshi Kuroiwa and Hiroshi Kumagai

Kashima Space Research Center, Communications Research Laboratory, Kashima, Ibaraki, Japan

1. INTRODUCTION

The information on clouds in terms of the heights of their bases and tops, the role and nature of layers in their structure, and vertical profiles of their water content (including whether it is liquid or ice) are all essential in studying the role of clouds in Earth's radiation budget [1]. The cloud profiling radar (CPR) which uses millimeter wavelengths can measure vertical distribution of cloud. CPR is sensitive enough to detect small cloud particles. Aribome CPR with scanning antenna can measure three-dimensional profiles of cloud. Three-dimensional profiles of the radar reflectivity in clouds are obtained from which profiles of the liquid water content (LWC) and ice water content (IWC) can be estimated. The size of cloud particles, an important property for the study of radiation, can not be estimated from CPR measurements alone but can be determined by combining CPR measurements with measurements from other sensors (for eaxmple, lidar or microwave radiometer).

With a view towards application in satellite-borne CPR, the Communications Research Laboratory (CRL) has developed an airborne W-band CPR which operates at 95 GHz, named SPIDER (Figure 1). On of the objectives of the development of SPIDER is evaluation and verification of 95-GHz radar technology. The data acquired from airborne radar measurements with SPIDER is used the development of algorithms for observation from space. The results from multiparameter measurements will be contributed to research on cloud radiation processes, cloud micro-physics, and clouds and precipitation.

SPIDER is primarily intended as a step toward future satellite-borne CPR system. This paper describes SPIDER's technical aspects and examples of data that have been obtained as a preliminary result.

2. DESIGN CONSIDERATION

In the Rayleigh regime, that is, the range of conditions in which the target particles are much smaller than the radio wavelength, the radar reflectivity factor depends on the particle distribution alone. The radar reflectivity factor Z is defined as follows by D: Particle diameter, N(D): Particle size distribution

$$Z = \int N(D) D^6 dD \qquad (1).$$

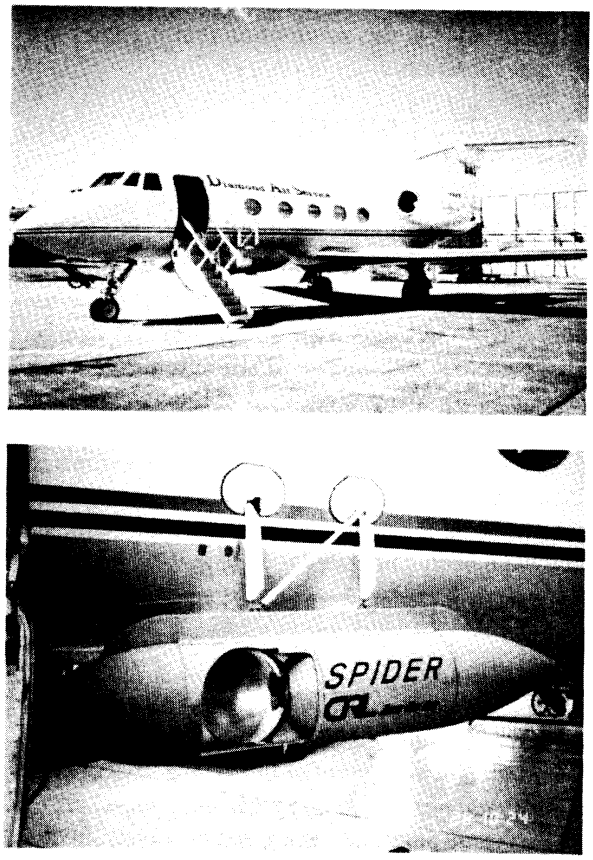

Figure 1 The aircraft and radar pod
(top panel) Aircraft with the SPIDER radar pod attached
(bottom panel) Radar pod with antenna reflector

* Corresponding author address: Hiroaki Horie, Kashima Space Research Center, Communications Research Laboratory, Hirai 893-1, Kashima, Ibaraki 314-0012, JAPAN; E-mail: horie@crl.go.jp

As can be seen in (1), the dimension of Z is the sixth power of length (mm^6/m^3). The relation between Z and the radar reflectivity η (m^{-1}), which is the average backscatter cross-section of the target per unit volume, is:

$$\eta = \frac{\pi^5 |K|^2}{\lambda^4} Z \qquad (2).$$

One of difficulties in measuring cloud particles with radar is the weak power that is scattered back from cloud particles. One solution to this problem is to use short millimeter wavelengths. As can be seen in (2), η is proportional to the inverse fourth power of λ. Hence, higher radar frequencies enable higher sensitivities. This increase in sensitivity is called the "Rayleigh gain". The Rayleigh gains are 39 dB and 22 dB for the W- and Ka-bands respectively, as compared using X-band radar.

LWC and IWC are important physical parameters for water clouds and ice clouds, respectively. On the assumption that particles are sphere, these are:

$$M = \frac{\pi\rho}{6 \cdot 10^6} \int_0^\infty D^3 N(D) dD \qquad (3),$$

where M represents the LWC or IWC (g/m^3) for water or ice clouds, respectively. ρ is the density of water or ice. If the particle size distribution in the cloud is given, M has a one-to-one correspondence with Z, and thus Z can be observed by radar. The distribution has been measured by using combined sensor techniques, such as combinations of radar and lidar, and radar and radiometer [2]. M can be estimated from radar measurements alone, using the empirical M-Z relations. Examples of relations that have been calculated to date are:

$$Z = 0.068 M^{1.9} \text{ (water cloud [3])} \qquad (4),$$

and

$$Z = 114.1 M^{1.44} \text{ (ice cloud [4])} \qquad (5).$$

Although both the Ka- and W-bands are near the center of atmospheric windows, their attenuation when propagating in the atmosphere is still not negligible. Clouds, and water vapor and oxygen, attenuate such radio waves. In the Rayleigh regime, the degree of attenuation by water clouds depends on M (LWC). The attenuation k that is specifically due to water clouds is:

$$k = 0.434 \cdot \frac{6\pi}{\lambda} \mathrm{Im}(-K) M \quad \text{(dB/km)} \qquad (6)$$

where the wavelength λ is in meters (6). We need to double the value of k given in (6) because the path of propagation for radar is both to and from the target. For a typical case with M=0.5 g/m^3, k at 95 GHz is about five dB for a one-km range (both send and return paths). Attenuation by ice clouds, however, is generally negligible, unless the ice cloud is very large.

Polarimetric radar observation is important for estimating the phase and shape of cloud particles. In atmospheric radar observation, the following parameters are commonly used in polarimetric observation, and to extract target properties. These parameters are derived from the covariance of elements of the scattering matrix S. The parameters, as laid out by Doviak and Zrnic [5], are:

a. radar reflectivity factor for the horizontally or vertically polarized component,

$$Z_h = \frac{4\lambda^4}{|K|^2 \pi^4} \left\langle |S_{hh}|^2 \right\rangle \qquad (7a)$$

$$Z_v = \frac{4\lambda^4}{|K|^2 \pi^4} \left\langle |S_{vv}|^2 \right\rangle \qquad (7b)$$

b. differential reflectivity,

$$Z_{DR} = 10 \log \frac{\left\langle |S_{hh}|^2 \right\rangle}{\left\langle |S_{vv}|^2 \right\rangle} \qquad (8)$$

c. linear depolarization ratio (LDR),

$$LDR = 10 \log \frac{\left\langle |S_{hv}|^2 \right\rangle}{\left\langle |S_{vv}|^2 \right\rangle} \qquad (9a),$$

or,

$$LDR = 10 \log \frac{\left\langle |S_{vh}|^2 \right\rangle}{\left\langle |S_{hh}|^2 \right\rangle} \qquad (9b),$$

d. co-polarized correlation coefficient,

$$\rho_{hv}(0) = \frac{\left\langle S_{vv} S_{hh}^* \right\rangle}{\left\langle |S_{hh}|^2 \right\rangle^{1/2} \left\langle |S_{vv}|^2 \right\rangle^{1/2}} \qquad (10),$$

e. differential phase,

$$\Phi_{DP}(r_0) = 2 \int_0^{r_0} [k_h(r) - k_v(r)] dr + \delta(r_0) \qquad (11),$$

where, k_h, k_v are the H and V propagation constants and δ is difference backscattered phase.

3. SYSTEM SPECIFICATION

The basic concept of SPIDER measurement is to simulate satellite measurements by flying above target clouds. SPIDER thus needs to be aboard an aircraft. The Gulf Stream II jet aircraft was selected to carry SPIDER for the experiment flights. The observation altitude is about 6000 m to 13000 m and the observation speed is about 100 to 200 m/s. The major parameters of the SPIDER system are listed in Table 1. The W-band frequency is selected to make smaller compact system than that of Ka-band radar.

Table 1 Specification of SPIDER

Frequency	95.040 GHz
Antenna aperture	40 cm
Antenna beam width	0.6 degree
Antenna gain	49.3 dBi(H), 49.5 dBi(V)
EIK transmitting power	1600 W
Maximum duty cycle	0.01 (1%)
Pulse width (PW)	0.25, 0.5, 1.0, 2.0 μ sec
Receiver noise figure	5.0 dB
Receiver dynamic range	75 dB
Pulse sequence	1, 4 or 6 sequences
Pulse spacing time	free (more than 100 times of PW)
Transmitting polarization	H or V (decided hit by hit)
Receiving polarization	H and V (simultaneously)
Pulse pair processing	realtime
FFT processing	realtime
Antenna scanning	-40～95° (for cross-track)
Polarization axis rotation	-45～45°

The antenna and RF sub-systems of the radar are housed in a pod attached outside the fuselage of the aircraft. The radar antenna can be directed at any inclination from the nadir to the horizon. Fig. 2 (top and bottlom panel) are photographs of the aircraft and radar pod. The SPIDER has the two type of the drive mechanism in the radar pod. One can be rotated with the antenna pointing in the plane perpendicular to track direction of aircraft (cross-track direction). The other can be rotated the polarization axis in a fixed antenna pointing. The antenna can be scanned over a range wider than that is required to scan from nadir to horizon. Polarization can be rotated ±45°, for calibration mainly. The horizontal and vertical polarization is defined when antenna is pointed to horizon and the angle of polarization axis is 0°.

-30dBZ has been used as a target sensitivity for satellite-borne CPR, but the value has no concrete basis. An assessment of the application of this value to the measurement of cirrus clouds has stated that 84 % of total cloud can be detected in the mid-latitudes [6]. Another report has stated that 99 % of cirrus can be detected [1]. One of objectives of SPIDER measurement is to evaluate this criterion for a satellite system. Therefore, SPIDER is much more sensitive than –30 dBZ over a 5-km range. The confirmation of sensitivity is important for the evaluation and verification of W-band radar rechnology.

Multiparameter radar measurements are very useful for the study of cloud radiation and microphysics. Both Doppler and polarimetric functions are implemented in SPIDER. Doppler measurement allows the cloud to be separated from precipitation (in most cases, the separation of drizzle from the water in the cloud is important). The size of raindrops as derived from their velocity of fall, and wind speeds, can also be obtained from Doppler data. It is not easy, however, to separate the vertical wind component from the velocity with which a particle falls. Polarimetric measurement allows discrimination between water and ice clouds, and determination of the shape of ice particles. Also, some information on cloud microphysics can be retrieved from differential phase measurement between two polarizations.

Even if the multiparameter radar functions are applied, further cloud parameters are still necessary. Among them, the size of particles in the cloud is particularly important, and cannot be obtained by radar measurement alone. Additional sensors are planned for the aircraft to allow the size of particles to be determined. Instruments for the measurement of radiation at visible and infrared wavelengths are housed in another pod which is attached to the other side of fuselage. During operation of SPIDER from a ground base, a lidar and microwave radiometer were available at a nearby site.

4. RADAR OPERATION

SPIDER has various operational patterns for both airborne and ground-based measurements, to accommodate the objectives of the experiment. The pulse train technique which has recently been developed as an element of multiparameter rain radar technology, is applied by SPIDER. The radar transmitter pulse consists of a series of pulses in a group (a pulse train). Correlations are processed by using appropriate combinations of pairs of pulses within a single group. The processed results are accumulated (or integrated) over the series of pulses in the train. The received power of the polarized signal components, processing of pulse pairs to obtain the Doppler velocity and its variance, the differential phase, and the correlation between two co-polarized components are all obtained by real time processing.

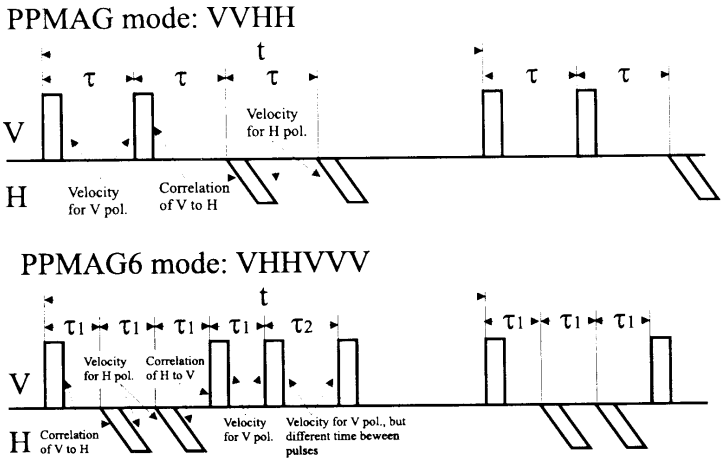

Figure 2 Example pulse trains
(a) The pulse train "VVHH" for PPMAG mode
(b) The pulse train "VHHVVV" for PPMAG6 mode
PPMAG mode and PPMAG6 mode are used to obtain the magnitude of both co-polarized and cross-polarized returned signals, and the pulse-pair components of the signal. The transmitted pulse sequence (a) consists of four pulses, and (b) consists of six pulses. "t" is the time for one cycle of the pulse train, "τ" and "τ_1" are the time intervals between pulses, and "τ_2" is a different time interval, to produce a staggered pulse. Staggered PRT (pulse repetition time) is used to increase the unambiguous velocity.

Examples of two transmitter pulse trains that are used in SPIDER are shown in Fig. 2, (a) and (b): pulse train (a) consists of four pulses (PPMAG), while (b) consists of six pulses (PPMAG6). In both cases the pulse width, polarization, and pulse interval of each pulse can all be set via software. In example (a), the received power for V and H polarization is obtained from log detection of all four pulses. The average and variance of the Doppler velocity are obtained by processing the first and second (or third and fourth) pulses. The coefficient of the correlation between the two co-polarized signals is obtained from the second and third pulses. In example (b), the phase shifts from V to H and H to V are obtained from the first and second pulses, and third and fourth pulses, as the respective pairs. A technique of staggering the pulse repetition time is applied by changing the pulse interval (between the fifth and sixth pulses in this example) to increase the composite unambiguous velocity [5].

5. EXAMPLE OBSSERVATION RESULTS

5.1 Results for ground observation

The first example SPIDER measurement is shown in Fig. 3, an observation from the ground at CRL's Kashima Space Research Center on 28 March 1999. The antenna is pointed at the zenith to take a vertical range profile. The upper panel shows the radar reflectivity factor Z, and the bottom panel shows Doppler velocity in vertical direction. The Doppler velocity is only plotted for points at which the received power was higher than –95 dBm. The two dimensional pattern of color in each panel shows the vertical distribution over an elapsed time of 160 s. The operating parameters for the radar are shown in the figure caption. The subtraction of noise power is performed for Z in order to improve sensitivity. The thin vertical stripes running from 3 to 10km in altitude are appeared, but they are not true signal. They are indicated failure of noise subtraction. The data has not been adjusted to compensate for attenuation in the atmosphere. Relatively few pulses were integrated in this case (264) and a very high sensitivity was not intended. However, clouds with a reflectivity of around –30 dBZ do appear in the near range of the plot.

Three cloud layers can be recognized in the upper panel that depicts Z. During this experiment, observers couldn't see upper and middle layers because the thick bottom layer of cloud was blocked. The bottom layer of stratus cloud appears below an altitude of 1 km. The

Doppler velocity in this layer is nearly constant at a small negative value (i.e. downward) over the period of observation. They are not ground clutter because any meaningful signal is not recognized at near range when it is no cloud, but that image is not shown. There is a middle-layer between about two and four km, and the reflectivity of these clouds is in the range between –20 and –10 dBZ. The Doppler velocity indicates downward motion in this layer, too. One interesting feature is that the areas with large negative velocities (up to the maximum of -3 m/s) correspond to the areas with larger values of Z. Although the velocity of the vertical background wind is unknown, it is reasonable to suggest that these areas reflect the velocity of fall for larger cloud drops. There is an upper layer of cloud above an altitude of seven km which consists of cirrus clouds. The Doppler velocity in this layer is in the low negative range. The slightly greater downward velocity that can be seen at the bottom of the layer represents the common tendency for cirrus clouds to contain relatively large ice particles.

5.2 Ground observation with antenna scanning

Fig. 4 shows the measurement from ground same as Fig. 3, but antenna is scanning over -15 to 60 degrees from zenith on 26 March 1999. The upper panel shows the radar reflectivity factor Z, and the bottom panel shows Doppler velocity in vertical direction. The operating parameters for the radar are shown in the figure caption. The subtraction of noise power is performed for Z in order to improve sensitivity. The stripes are running radially in the upper panel of Fig. 4. They are also indicated failure of noise subtraction due to too small number of averaging.

This figure shows two-dimentional cross section cut out from actual three-dimentional distributed cloud over ten km wide range at 4 km to 12 km altitude. Three layers are recognized in this figure. The bottom layer is thick cloud and altitude is under the one km. The middle layer is very thin cloud at about 4 km altitude. The received signal from this layer is weak but meaningful Doppler velocity are recognized. The top layer has the complex structure. There are multi-layers in this layer itself.

From the radial Doppler velocity (bottom panel of Fig. 4), the existence of horizontal wind at each layer is assumed. The Doppler velocity at left side of bottom layer is positive, then it is moved to negative at the right side. The wind direction is assumed right to left. At the top layer, the direction of moving is opposite. The Doppler velocity is move from positive to negative (color indicated red to blue) at the right side of top layer. It is indicated that the folding of Doppler velocity is occurred. The wind direction is assumed left to right.

5.3 Airborne observation results

Fig. 5 is a set of images obtained during airborne observation. The antenna is directed towards the nadir and vertical range profiles thus obtained are from the aircraft down. The data was obtained above the Japan Sea off the shore of Niigata Prefecture, on 15 June 1999. The three panels from the top to bottom show the patterns for Z, the Doppler velocity and LDR. The vertical and horizontal axes represent distance from the aircraft, and horizontal distance traveled in flight, respectively. The subtraction of noise power is also performed for Z. The thin vertical stripes running from 6 to 12km in range are indicated failure of noise subtraction. A layer of ice cloud can be seen at altitudes above five to six km in the distribution of Z (top panel). The almost perfectly horizontal white line at the 12 to 12.5-km range is the echo from the surface of the sea, and its intensity is of course much higher than that for a typical cloud.

The highest values of Z appear in the bottom part of the cloud layer. The boundary at the cloud base contains some structural features that are smaller than one-km across. The Doppler velocity shown in the middle panel has been corrected for the effects of aircraft attitude and vibration, by adjusting the values relative to a velocity of zero for the surface of the sea. Cell-like structures appear at the bottom of the cloud and correspond to the equivalent features in the pattern for Z. There are areas of high velocity, both negative and positive, in a pattern which appears somewhat periodic. The bottom panel shows values of the LDR, and for the cloud it is mainly close to or less than –30 dB, or could not be defined properly because the cross-polarization signal is below the receiver noise level. Hence, for most of the area shown, the LDR is meaningless. Nevertheless, it is remarkable that layers with high LDR (above -25 dB) can be seen near the cloud bottom at horizontal distances of 51–55 km. This would appear to indicate the presence of ice particles with a high degree of eccentricity, which in general means particles of a larger size. The area

with a large negative Doppler velocity in the middle panel may correspond to this region.

5.4 Sea surface echo

We will discuss the echo from the surface of the sea, which can clearly be seen in the top and middle panels of Fig 5, in more detail. The upper panel of Fig. 6 shows the received power against range, for the region close to the surface of the sea. The bottom panel shows the peak received power values for the echo from the surface of the sea. The horizontal axis indicates distance and covers over 50 km of the flight. The data was obtained along the same flight path as that which is shown in Fig. 5, but a greater distance is shown. In the upper panel of Fig. 6, the range of the echo from the surface of the sea increases with distance, which represents the ascent of the aircraft. The peak level is almost constant except for a slight decrease over distance, between zero and 30 km. This gradual decrease in the peak level is consistent with the increase in range. After 30 km, the level is lower than that which would be extrapolated from the earlier values, and the level is itself variable. These data indicate that the level of the echo from the surface of the sea can be constant in some cases, when the effects of attenuation by clouds and atmospheric gases are negligible or constant, even in the W-band. At the higher distances shown in Fig. 6, the level of attenuation due to clouds increases and becomes quite variable.

The reason for this discussion in some detail is because the echo from the surface of the sea has potential as a reference level for radar calibration in future airborne or satellite-borne cloud radar measurements in the W-band. In satellite data for the TRMM (Tropical Rainfall Measuring Mission), the echo from the surface of the sea is an important reference source that is used to correct for attenuation by rain, and to calibrate the radar at a frequency of 13.8 GHz [7]. In the W-band, reliable information on the radar cross-section and signature of the surface of the sea has yet to be reported. SPIDER's future observations will pioneer this area and provide information with a potential application to the calibration of future satellite-borne cloud radar.

6. CONCLUSION

The airborne cloud profiling radar (SPIDER) was developed at CRL, then the objetives and design considerations are described. SPIDER provides very high sensitivity to small cloud particles. The radar is carried by a jet aircraft that can fly high above most clouds. Other features of SPIDER are to provide the capable to observe the cloud by full-polarimetric and Doppler measurements. The radar is still undergoing performance testing and preliminary test results are given in the current paper. The current conclusions are that the SPIDER system functions are working as intended, and that the system is quite capable in terms of cloud measurement. In this paper, the data indicate the features of SPIDER are shown. The plan of joint measurement with lidar and/or micro-wave radiometer is undergoing. These measurements will be contributed to determine size distribution. We hope that the development of, and results from, SPIDER will contribute to the realization of satellite-borne cloud radar and the advance of cloud science research.

References

[1] P. R. Brown, A. J. Illingworth, A. J. Heymsfield, G. M. McFarquhar, K. A. Browning, and M. Gosset, "The role of spaceborne millimeter-wave radar in the global monitoring of ice cloud", J. Appl. Meteor., vol.34, pp. 2346-2366, 1995.

[2] S. Y. Matrosov, A. J. Heymsfield, R.. Kropfli, B. E. Martner, R. F. Reinking, J. B. Snider, P. Piironen, and E. W. Eloranta, "Comparison of ice cloud parameters obtained by combined remote sensor retrievals and direct methods", J. Atmos. Ocean. Technol., vol.15, pp.184-196, 1998.

[3] H. Sauvageot and J. Omar, "Radar reflectivity of cumulus clouds", J. Atmos. Ocean. Technnol., vol.4, pp. 264-272, 1987.

[4] K. Sassen, "Ice cloud content from radar reflectivity", J. Climate Apllied Meteor., vol.26, pp.1050-1053, 1987.

[5] R. J. Doviak and D. S. Zrnic, *Doppler Radar and Weather Observation*, 2nd Ed., Academic Press., 1993.

[6] D. Atlas, S. Y. Matrosov, A. J. Heymsfield, M-D Chou, and D. B. Wolf, "Radar and radiation properties of ice clouds", J. Appl. Meteor., vol.34, pp. 2329-2345, Nov. 1995.

[7] T. Kozu, T. Kawanishi, H. Kuroiwa, M. Kojima, K. Oikawa, H. Kumagai, K. Okamoto, M. Okumura, H. Nakatsuka, and K. Nishikawa, "Development of precipitation radar onboard the Tropical Rainfall Measuring Mission (TRMM) satellite", submitted to IEEE Trans. Geosci. Remote Sens., 1999.

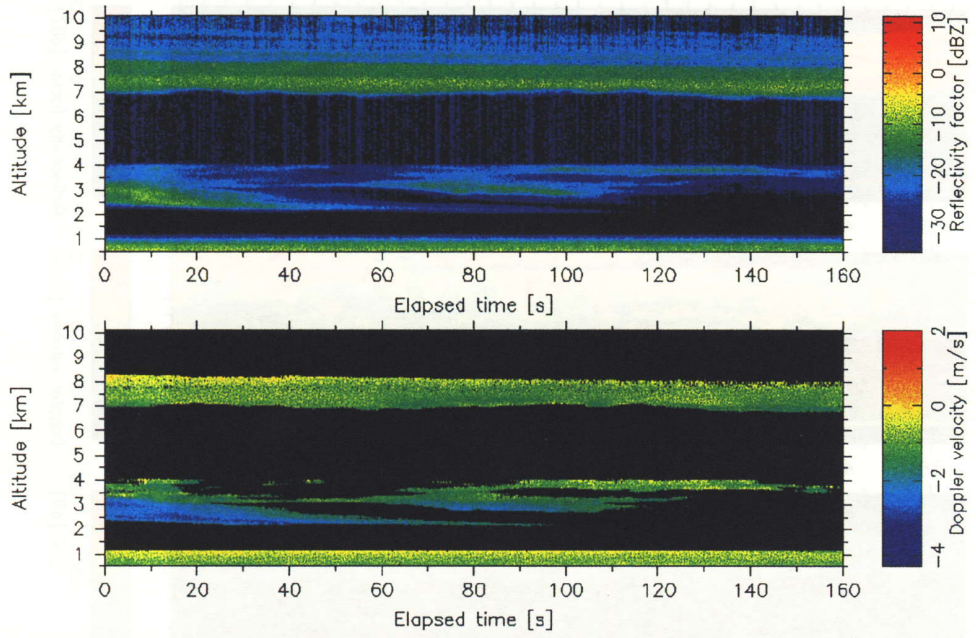

Figure 3 Cloud images obtained from the ground with zenith looking antenna, on the 28th Mar., 1999
(top panel) Radar reflectivity factor (Z) (bottom panel) Doppler velocity (V_D)
The image was obtained using PPMAG mode: i.e. "VVHH" and a 0.5-μsec pulse width. The number of averaging pulses was 264. The subtraction of noise power is performed in (top panel). Positive velocities are upward motion in (bottom panel). Black indicates that data was not available because reflectivity was too low.

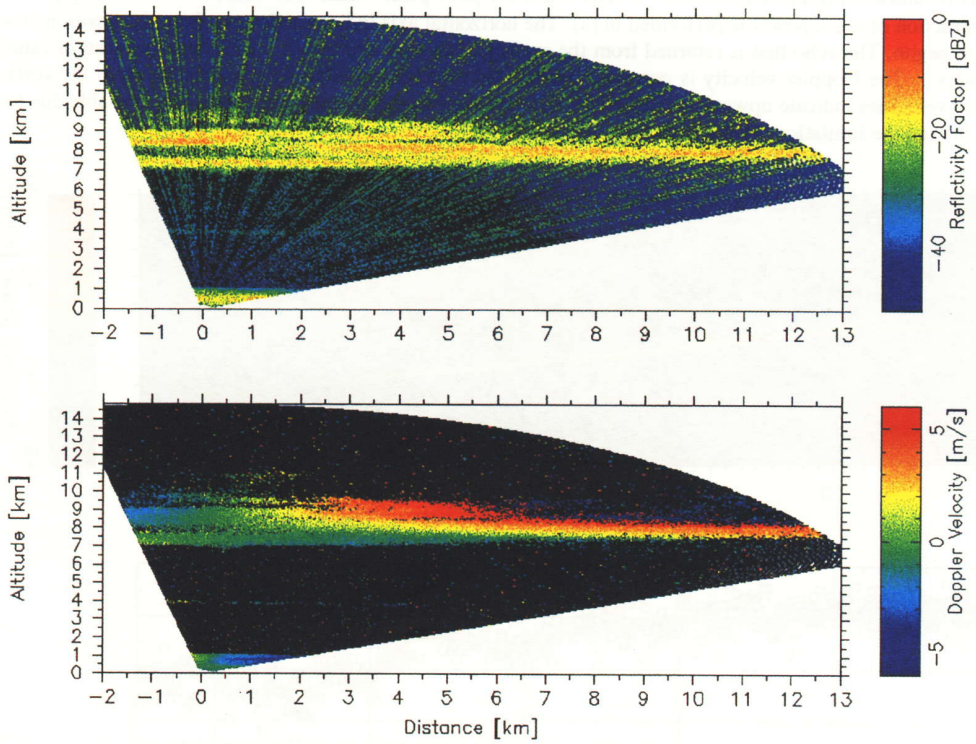

Figure 4 Cloud images obtained from the ground with antenna scanning, on the 26th Mar., 1999
(top panel) Radar reflectivity factor (Z) (bottom panel) Radial doppler velocity (V_D)
The image was obtained using PPMAG mode: i.e. "VVHH" and a 0.5-μsec pulse width. The number of averaging pulses was 28. The subtraction of noise power is performed in (top panel). Positive velocities are away from radar (bottom panel). Black indicates that data was not available because reflectivity was too low.

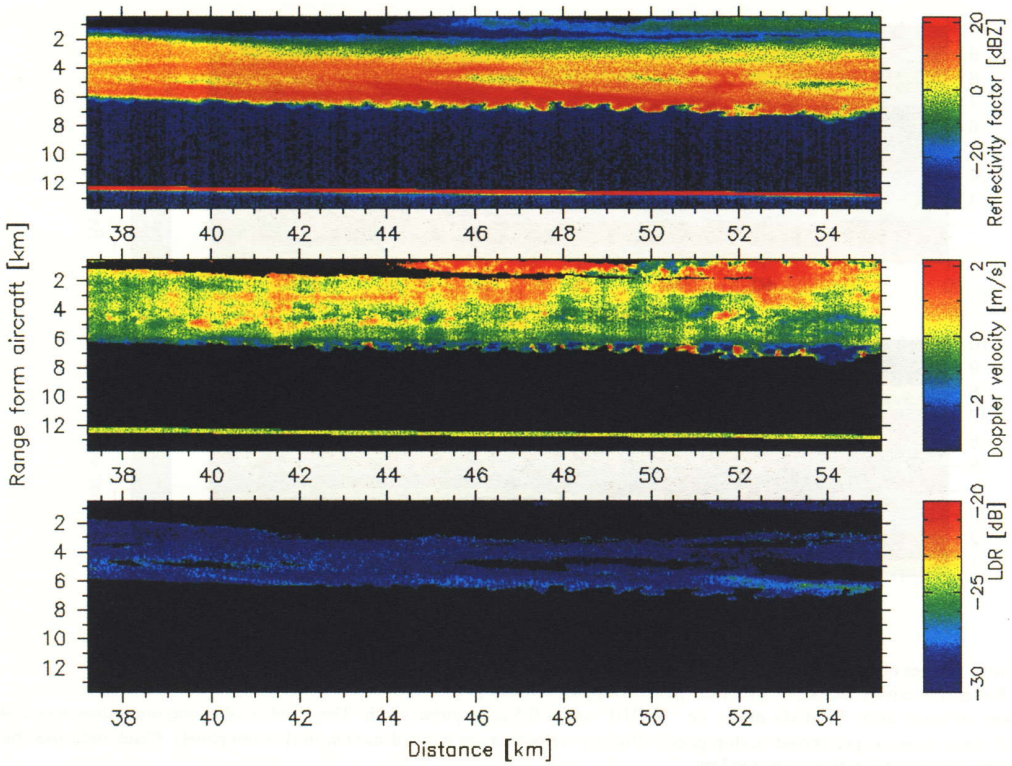

Figure 5 Cloud images obtained by airborne measurement with nadir looking antenna, on the 15th Jun., 1999
(a) Radar reflectivity factor (Z) (b) Doppler velocity (V_D) (c) L_{DR} (Linear depolarization ratio)
The image was obtained using PPMAG mode: "VVHH", and a 1-μsec pulse width. The number of averaging pulses was 176. The subtraction of noise power is performed in (a). The horizontal axis indicates distance from the position at which data acquisition begun. The echo that is returned from the surface of the sea appears as a white line because of saturation of the color index. The Doppler velocity is corrected against the velocity indicated by echo returns from the surface of the sea. Positive velocities indicate upward motion in (b). Black in the image indicates that data is not available due to: low reflectivity in (b) and the limitation arising from the noise level in (c).

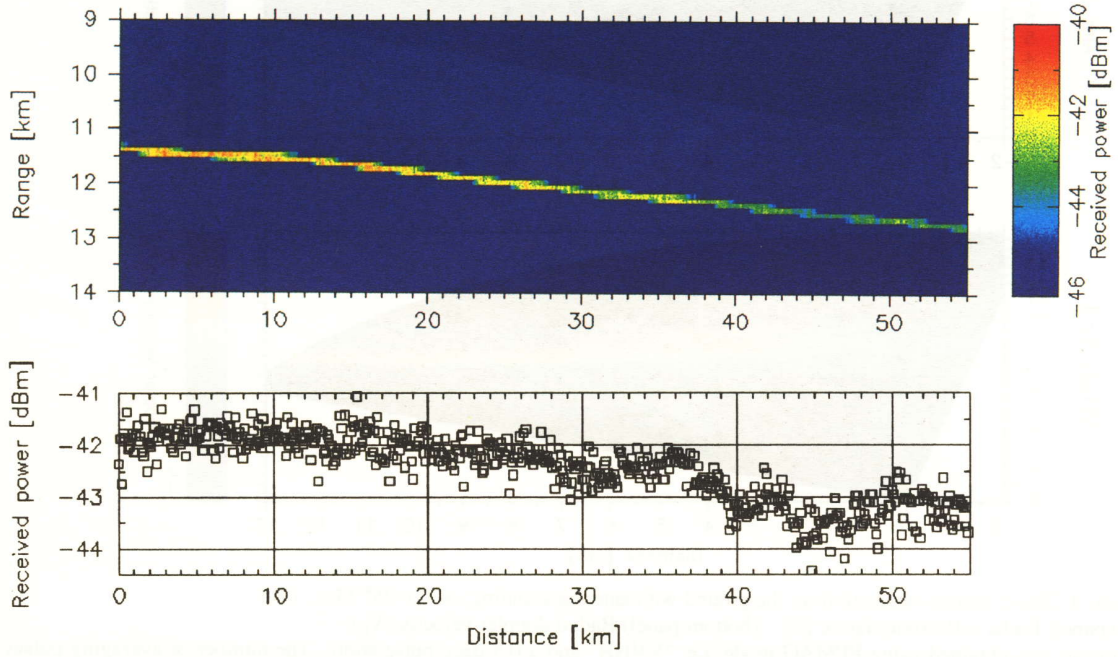

Figure 6 The received power from the sea surface for observation from the aircraft in the direction of the nadir
(a) Enlarged radar image in the range around the surface of the sea
(b) Plot of peak level at the surface of the sea.
The data is the same as is shown in Figure 5, but for a longer portion of the flight, and the number of averaging pulses is 880. The horizontal axis is also the same as in Figure 5.